Polymer 110 (2017) 1–11

Contents lists available at ScienceDirect

Polymer

journal homepage: www.elsevier.com/locate/polymer

Selective distribution and migration of carbon nanotubes enhanced electrical and mechanical performances in polyolefin elastomers

Tao Gong [a], Meng-Qi Liu [a], Hu Liu [b], Si-Piao Peng [a], Ting Li [a], Rui-Ying Bao [a], Wei Yang [a, *], Bang-Hu Xie [a], Ming-Bo Yang [a], Zhanhu Guo [b, **]

[a] College of Polymer Science and Engineering, State Key Laboratory of Polymer Materials Engineering, Sichuan University, Chengdu 610065, Sichuan, China
[b] Integrated Composites Laboratory (ICL), Department of Chemical & Biomolecular Engineering, University of Tennessee, Knoxville, TN 37996, USA

ARTICLE INFO

Article history:
Received 2 November 2016
Received in revised form
13 December 2016
Accepted 21 December 2016
Available online 23 December 2016

Keywords:
Double percolation
Reduced percolation threshold
Electrical conductivity

ABSTRACT

A thermodynamic and kinetic method based on the selective distribution and migration of multi-walled carbon nanotubes (MWCNTs) in polyoxyethylene (PEO)/ethylene-α-octene random copolymer (ORC) composite system was reported to improve the dispersion of MWCNTs in ORC. Scanning electron micrographs and transmission electron micrographs confirmed that MWCNTs could almost completely migrate from the PEO phase to the ORC phase during melt compounding and lead to tremendously improved dispersion of MWCNTs in ORC, compared with traditional melt compounded ORC/MWCNT composites. Rheological analysis revealed that better MWCNTs network was developed at a lower content of MWCNTs with an improved dispersion of MWCNTs in ORC. The percolation threshold was drastically reduced from 3.82 to 0.35 vol % and the electrical conductivity was tremendously improved. The mechanical properties were also fully enhanced in comparison with traditional melt compounded ORC/MWCNT composites owing to the homogeneous dispersion of MWCNTs. These results manifest that, by proper selection of components with a selective distribution of MWCNTs and controlling the migration process of MWCNTs in the composites, the dispersion of MWCNTs in polymer matrix and resulting performance of the nanocomposites can be greatly improved.

1. Introduction

Electrically conductive polymer composites (CPCs) have demonstrated unique properties including low density, good processability, corrosion resistance and adjustable electrical conductivity [1–4] and have been applied in the fields of sensors, capacitors, stretchable electronics and conductive adhesives [5–8]. One of the most commonly studied and applied methods to fabricate CPCs is introducing electrically conductive ingredients such as carbon black (CB), carbon nanotubes (CNTs) or graphene into a polymer matrix [9–12]. CNT is an ideal conductive ingredient because of its unprecedented physical and chemical properties, excellent conductive and mechanical performance [13]. However, homogenous dispersion of CNTs in polymer matrix is generally hard to be achieved because of their strong interactions and entanglements resulting from the large specific surface area and high aspect ratio of CNTs [14–16].

Numerous studies have been carried out for improving the dispersion of CNTs in polymer matrix via a variety of approaches [17,18], by ways of using special mixing methods [19,20] (*e.g.* ultrasonic treatment, high speed shearing, coagulation method, *etc.*), functionalization of CNTs [21,22] (*e.g.* purification, chemical functionalization, activation treatment, *etc.*), modification of polymer matrix [14], utilization of surfactant and compatibilizer [23], *in situ* polymerization [24] and other sophisticated methods [17,25,26]. For example, Bryning et al. [19] developed a methodology to disperse purified single-walled carbon nanotubes (SWCNTs) into epoxy with ultrasonic treatment and significantly reduced the percolation threshold. Roy et al. [21] reported a highly homogeneous dispersion of multi-walled carbon nanotubes (MWCNTs) in nylon 12 matrix by grafting 2-acrylamido-2-methylpropane sulfonic acid (AMPS) onto MWCNTs via ultraviolet/ozone (UV/O_3) assisted polymer grafting and the dispersion of MWCNTs was improved to a certain extent. Nevertheless, due to the complicated operations, harsh reaction conditions, high cost or the utilization of toxic solvents, most of these methods cannot be deployed for

* Corresponding author.
** Corresponding author.
E-mail addresses: weiyang@scu.edu.cn (W. Yang), zguo10@utk.edu (Z. Guo).

http://dx.doi.org/10.1016/j.polymer.2016.12.056
0032-3861/

industrial productions.

The introduction of conductive fillers into polymer blends offers a way for the development of conductive composites with lower filler concentrations [27,28]. The localization of fillers in polymer blends is determined by the interplay between thermodynamic driving force and kinetic factors [29–31]. Therefore, nonequilibrium filler localization states can be obtained, especially if the particle is initially localized within the thermodynamically less favorable phase of the blends. As a result, the migration of fillers such as CNTs in polymer blends was frequently observed during melt compounding [30,32,33]. For instance, Göldel et al. [34–36] reported the migration process of CNTs in polycarbonate/poly(styrene-acrylonitrile) (PC/SAN) blends during melt mixing in terms of both thermodynamics and kinetics and found that because of the high aspect ratio, CNTs were more likely to migrate into a more thermodynamically favorable phase rather than distribute at the interface of the blend. Although the migration method has led to greatly improved electrical performance of polymer composites based on polymer blends and CNTs, the homogenous dispersion of CNTs in polymer via a migration strategy has not been reported.

Elastomeric conductive composites have attracted enormous attention recently because of their high and reversible deformability and persistent conductive pathways when stretched, twisted or folded [37–40]. With well-defined structures, homogeneous comonomer distribution, narrow molecular weight distribution and adjustable molecular weight, ethylene-α-octene copolymers (EOCs) are considered as one of the most widely used elastomeric polymers [41–43]. However, in our previous work on polyolefin elastomer composites, the dispersion of MWCNTs was found to be greatly different in EOCs with different chain architectures (ethylene-α-octene random copolymer (ORC) and ethylene-α-octene block copolymers (OBC)). We found that MWCNTs were dispersed extremely uniform in OBC and seriously aggregated in ORC, and the electrically conductive performance of ORC/MWCNT composites was poor and the percolation threshold was up to 9 vol% [44]. Aiming at improving the conductive performance of ORC/MWCNT composites, a novel segregated structure with the chemically cross-linked ORC particles working as the segregating particles was constructed for ORC/MWCNT composites [4] and the percolation threshold was significantly decreased together with greatly enhanced electrical conductivity and mechanical performance. However, the dispersion of MWCNTs in ORC matrix is still not improved. Furthermore, the porous structure arising from the removal the assisted polymer phase has not been reported yet.

In this work, an effective thermodynamic and kinetic method was developed to improve the dispersion of MWCNTs in polymer matrix with ORC as a model polymer. A water soluble polymer, polyoxyethylene (PEO) was adopted as an assistant phase. MWCNTs were found to be uniformly dispersed in PEO and in PEO/ORC blend, MWCNTs tend to be distributed in the ORC phase thermodynamically. First, PEO/ORC/MWCNT composites with a double percolation structure, in which MWCNTs were selectively distributed in PEO phase, were fabricated by melt compounding. With further melt compounding, MWCNTs migrated from the PEO phase to ORC phase. After a sufficient time and the finish of migration process, almost all MWCNTs migrated into the ORC phase from the PEO phase and uniform dispersion of MWCNTs in the PEO phase was transferred to the ORC phase. After the PEO phase was removed by deionized water, porous ORC/MWCNT composites were obtained. Then the porous ORC/MWCNT composites were melt processed again and a uniform dispersion of MWCNTs in ORC matrix was acquired and maintained. The uniformly dispersed MWCNTs can effectively construct an electrical conducting network in ORC matrix, leading to a significantly decreased percolation threshold, tremendously improved conductivity, and simultaneously enhanced mechanical performance of the composites, compared with conventional melt compounded ORC/MWCNT composites.

2. Experimental

2.1. Materials

ORC (ENGAGE 8150), with the weight average molecular weight of 162, 700 and a polydispersity of 2.1, was purchased from Dow Chemical Co. (Midland, MI, USA). PEO (P101340), with the number-average molecular weight of 300, 000, was purchased from Aladdin Biochemical Technology Co. Ltd. (Shanghai, China). MWCNTs (NC7000), with the average diameter of 9.5 nm and length of 1.5 μm, were purchased from Nanocyl SA Co. (Sambreville, Belgium). The density of MWCNT is 1.8 g/cm^3 and the TEM micrograph is shown in Fig. S1.

2.2. Sample preparation

Before melt compounding, the polymers were dried in a vacuum oven at 40 °C for 12 h. The melt compounding was conducted in a torque rheometer (XSS-300, Shanghai Kechuang rubber Plastics Machinery Set Ltd., China) at 140 °C. To ensure that MWCNTs migrate from the PEO phase to the ORC phase during melt compounding, the PEO pellets and MWCNTs were melt compounded in the torque rheometer at 50 rpm for 3 min firstly, and then ORC pellets were added and the mixture was continued to compound for another 15 min. After mixing, the blends were rapidly quenched in cold water to freeze the phase morphology. To obtain a co-continuous structure, the weight ratio of PEO and ORC was controlled to be 50/50 for all the blends and the obtained samples were named as PEO/ORC/MWCNT-X, where X represents the volume fraction of MWCNTs in the composites.

For completely removing the PEO phase in PEO/ORC/MWCNT-X, selective solvent extraction of the PEO phase in deionized water was performed in a beaker for one week. During the selective solvent extraction, the deionized water was changed and a 30 min ultrasonic treatment was carried out every 12 h. The energy input of sonication was fixed at 400 W. Then the samples were dried in a vacuum oven at 40 °C for 24 h to remove any residual deionized water.

After the PEO phase was selectively removed, the samples were compression molded again at 140 °C and 10 MPa for 5 min. The obtained samples were named as R-ORC/MWCNT-X, where X represents the volume fraction of MWCNT content in the R-ORC/MWCNT composites.

For comparison, conventional melt compounded ORC/MWCNT composites and PEO/MWCNT composites with different content of MWCNTs were also prepared by melt compounding in the same torque rheometer at 140 °C and 50 rpm for 15 min and these samples were marked as ORC/MWCNT-X, where X represents the volume fraction of MWCNTs in ORC/MWCNT composites.

2.3. Characterization

2.3.1. Contact angle measurements

Contact angle measurement were conducted with a drop shape analyzer (DSA100, KRÜSS Ltd., Hamburg, Germany). The measurements were performed in sessile drop mold at 25 °C with water and diiodomethane as the wetting solvents. PEO and ORC samples were compression-molded sheets at 140 °C for 5 min, and then cooled down to 25 °C under pressure for 2 min. Contact angles were measured on 3 μl wetting solvent at 25 °C, and the results were the average values of at least five replicates.

2.3.2. Morphology investigation

After the samples were cryo-fractured in liquid nitrogen and the fractured surface was coated with a thin layer of gold to avoid charge accumulation, the morphology of the samples was examined using a scanning electron microscopy (SEM, JEOL JSM-5900LV, Japan) operating at 20 kV. Furthermore, the dispersion states of MWCNTs at the microcosmic scale were also observed with a transmission electron microscope (TEM, Tecnai G2 F20s-TWIN, Germany) equipped with a field emission gun operating at 200 kV. The ultrathin samples with a thickness of 50–100 nm were cut on a Leica EM UC6 ultramicrotome (Leica Microsystems, Wetzlar, Germany) at −120 °C.

2.3.3. Rheological analysis

Rheological measurements were performed on a stress controlled dynamic rheometer (AR2000ex, TA Instruments, USA) equipped with 25 mm parallel plates. Disk samples for rheological analysis were compression-molded at 140 °C and 10 MPa for 5 min. The thickness and diameter of the samples were 1.5 and 25 mm, respectively. Dynamic frequency sweep was performed from 0.01 to 100 Hz at a strain of 0.1% within the linear viscoelastic region at 140 °C. To prevent thermal and oxidative degradation, all the tests were carried out under nitrogen atmosphere.

2.3.4. Resistivity measurements

Room temperature resistance (R) measurements were performed at 25 °C. When the R below 1×10^9 Ω, rectangular sheets of 30 mm in length, 10 mm in width and 2 mm in thickness for all samples were compression molded at 140 °C and 10 MPa for 5 min. Then the samples were measured by using a two-probe method with a digital multimeter (Keithley 6517B, Keithley, Ohio, USA). When the R was above 1×10^9 Ω, circular sheets of 100 mm in diameter and 1 mm in thickness for all samples were also prepared under the same condition. Then the samples were measured with a high-resistance meter (ZC360, Shanghai, China). For the sake of providing stable values of the resistivity, silver paste was evenly painted onto the surface of samples in contact with the probes of digital multimeter, to ensure good electrical contact.

2.3.5. Mechanical properties

The mechanical performance was determined on an AGS-J universal materials testing machine (the maximum capacity of the load cell was limited to 10 kN) at 25 °C with a gauge length of 20 mm. All the samples used for mechanical performance testing were dumb-bell samples with dimensions of 20 mm × 4 mm × 1 mm which were tailored from the circular sheets prepared previously. The uniaxial tensile fracture test was carried out at a crosshead speed of 100 mm/min. At least five samples were tested and the average results were reported.

3. Results and discussion

3.1. The dispersion of MWCNTs in PEO and ORC matrix

The dispersion of MWCNTs in PEO and ORC matrix were examined by SEM. Fig. 1 shows the SEM micrographs of the PEO/MWCNT composites and ORC/MWCNT composites. Obviously, extremely uniform dispersion of MWCNTs in the PEO matrix and no agglomeration are observed at low magnification, Fig. 1a, similar to the PEO/MWCNT composites in previous reports [45,46]. A great amount of individual MWCNTs are visible as indicated in Fig. 1c. In stark contrast, as shown in Fig. 1b and d, the aggregation of MWCNTs is serious in the ORC/MWCNT composites with huge MWCNT clusters randomly dispersed in the ORC matrix and there is almost no tiny MWCNT cluster in the MWCNTs sparse regions. Undoubtedly, ameliorating the awful dispersion of MWCNTs is the key to acquire high performance ORC/MWCNT composites.

When WMCNTs are introduced into immiscible polymer blends, they are usually distributed in one phase or at the interphase rather than homogeneously distributed in the whole polymer blends, depending upon the affinity to the polymer components [31,47,48]. Normally, the location of MWCNTs can be predicted by a wetting parameter (ω) proposed by Sumita et al. [49] and Fenouillot et al. [30]:

$$\omega_A = \frac{\gamma_{filler-B} - \gamma_{filler-A}}{\gamma_{A-B}} \quad (1)$$

where $\gamma_{filler\text{-}A}$ and $\gamma_{filler\text{-}B}$ are the interfacial tensions between the filler and polymer A and B, respectively, while $\gamma_{A\text{-}B}$ is the interfacial tension between polymer A and polymer B. If $\omega_A > 1$, the filler distributes in polymer A; if $\omega_A < -1$, the filler locates in polymer B; and if $-1 < \omega_A < 1$, the filler distributes at the interface.

The interfacial tension between two phases can be estimated from Equation (2) [50]:

$$\gamma_{1-2} = \gamma_1 + \gamma_2 - 2\sqrt{\gamma_1^d \gamma_2^d} - 2\sqrt{\gamma_1^p \gamma_2^p} \quad (2)$$

where γ is the surface tension, $\gamma = \gamma^d + \gamma^p$, γ^d is the dispersion component of surface tension, and γ^p is the polar component. The surface tension of the materials and interfacial tension between materials are listed in Table 1 and Table 2, respectively.

Taking PEO as polymer A, the calculated value of ω_A is $-1.14 < -1$, indicating that MWCNTs prefer to distribute in ORC phase of PEO/ORC blend thermodynamically.

3.2. The strategy to improve the dispersion of MWCNTs in ORC matrix

Fig. 2 gives a schematic diagram for improving the dispersion of MWCNTs in ORC matrix by using the uniform dispersion of MWCNTs in the PEO phase and the migration process of MWCNTs in the PEO/ORC blends. As shown in Fig. 2a, MWCNTs disperse uniformly in PEO and seriously aggregate in ORC. To obtain PEO/MWCNT composites with MWCNTs uniformly dispersed in PEO, MWCNTs were melt compounded with PEO first. Then the PEO/MWCNT composites were mixed with ORC by melt compounding. So, at the beginning of the melt compounding process, Fig. 2b, MWCNTs are selectively distributed and uniformly dispersed in the PEO phase of PEO/ORC blends and a double percolation structure can be obtained by controlling the content of components. According to the results of Equations (1) and (2), during melt compounding, MWCNTs tend to migrate from the PEO phase to the ORC phase [28,29,34,35], as illustrated in Fig. 2c. In the migration process, MWCNTs can maintain the form of isolated nanotubes from the PEO phase to the ORC phase. After a sufficient time and the finish of the migration process, almost all MWCNTs can migrate to the ORC phase from the PEO phase [34], as shown in Fig. 2d. Because MWCNTs can hold the form of isolated nanotubes during the whole migration process due to the weak interactions between MWCNTs with no functional groups on the tube surface, a uniform dispersion of MWCNTs in the ORC phase can be eventually achieved. According to literature reports [53–55], one phase in this co-continuous structure can be completely removed by using a suitable solvent. In this work, PEO is a water-soluble polymer and ORC cannot dissolve in water. As the PEO phase is selectively removed by water, in Fig. 2e, continuous porous PEO/MWCNT conductive composites can be acquired. Then the continuous porous ORC/MWCNT composites are compressed again on a compression

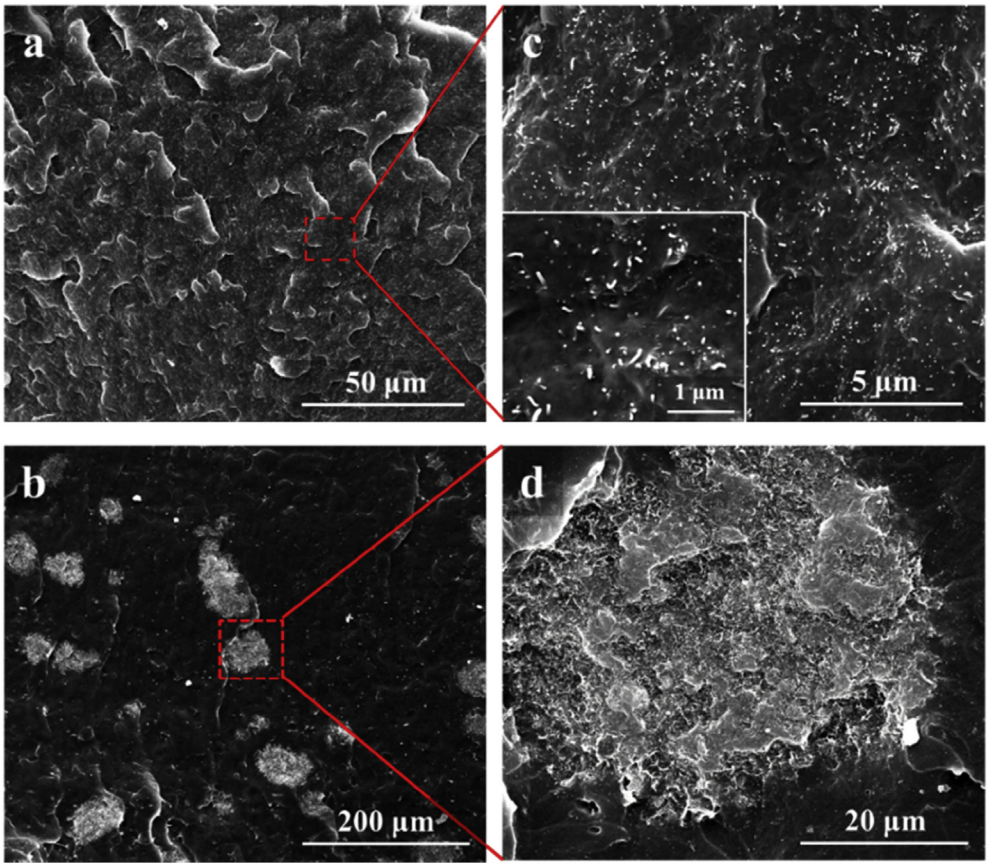

Fig. 1. SEM micrographs of (a) PEO/MWCNT-3.06 vol% and (b) ORC/MWCNT-2.20 vol%. Image (c) and (d) are the amplification of image (a) and (b) respectively, and the insert in (c) is the local amplification.

Table 1
Surface tension values of PEO, ORC and MWCNT.

Sample	Surface tension (mN/m)		
	γ	γ^d	γ^p
PEO	46.5	42.3	4.2
ORC	31.4	29.5	1.9
MWCNT[a]	27.8	17.6	10.2

[a] According to *Romain* et al. [51] and Baudouin et al. [52] and Taguet et al. [29].

Table 2
Interfacial tension values between each possible pair calculated by equation (2).

Possible pairs	PEO/MWCNT	ORC/MWCNT	PEO/ORC
Interfacial tension (mN/m)	6.64	4.82	1.60

molding machine at 140 °C. Finally, the R-ORC/MWCNT composites with an extremely uniform dispersion of MWCNTs in ORC matrix can be obtained as indicated in Fig. 2f.

3.3. The dispersion and migration of MWCNTs in PEO/ORC blends

The SEM micrographs of PEO/ORC/MWCNT composites experienced different time of melt compounding are shown in Fig. 3 to illustrate the migration of MWCNTs during melt compounding. Fig. 3a, c and e reveal the distribution of MWCNTs in PEO/ORC/MWCNTs composites after melt compounding for 1 min. The composites are not very homogenous at the initial stage of melt compounding, because the blending process has not reached the equilibrium state yet. Compared with the morphologies of PEO/ORC/MWCNT composites and the etched composites, it can be confirmed that MWCNTs are selectively distributed in the PEO phase and only a few single carbon nanotubes have migrated into the ORC phase. It is worth noting that there are many individual MWCNTs distributed at the interface and form a plurality of bridge between the two phases as shown in Fig. 3c. This indicates that MWCNTs tend to migrate from the PEO phase to the ORC phase, consistent with the thermodynamic prediction. The morphologies of PEO/ORC/MWCNT composites experienced 5 min melt compounding can be observed in Fig. 3b and d and f. After melt mixing for 5 min, the composites showed a co-continuous structure and MWCNTs were present in both the PEO phase and the ORC phase. Comparing Fig. 3c and f, the number of MWCNTs in the ORC phase significantly increased. This result clearly shows that MWCNTs can migrate from the PEO phase to the ORC phase during melt compounding. Because MWCNTs were initially localized in the PEO phase but revealed a comparable higher affinity toward the ORC phase. So, during the melt compounding, MWCNTs experienced a thermodynamic driving force toward the ORC phase. Hence, the thermodynamic driving force impelled MWCNTs to migrate from the PEO phase to the ORC phase.

Fig. 4a, c and e are the SEM micrographs of PEO/ORC/MWCNT composites experienced 15 min melt compounding. As can be seen in Fig. 4a, after melt compounded for 15 min at 140 °C, PEO/ORC/MWCNTs composites maintained a typical co-continuous structure and no aggregation of MWCNTs occurred. Fig. 4c and e are the partial enlarged view of Fig. 4a, where both the PEO phase and the ORC phase are included. It is worth noting that, the interface

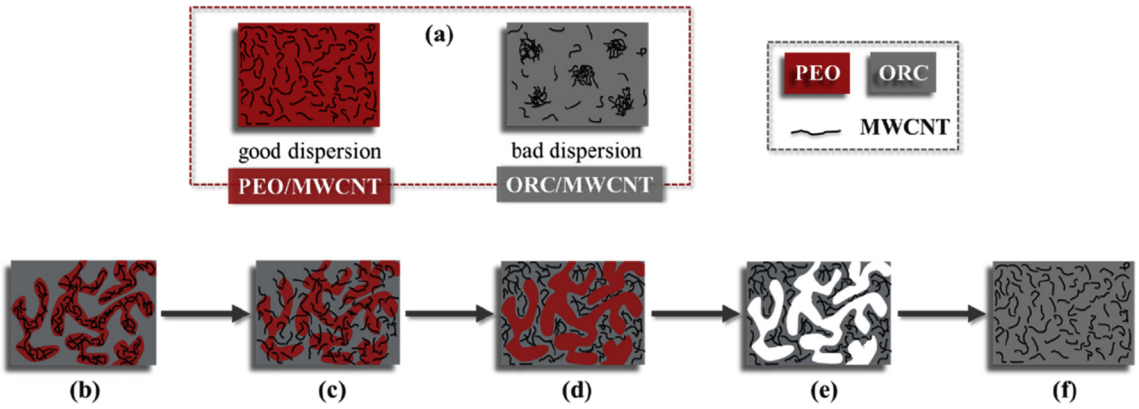

Fig. 2. Schematic diagram for improving the dispersion of MWCNTs in ORC matrix. (a) the dispersion of MWCNTs in PEO and ORC matrix; (b) MWCNTs uniformly disperse in the PEO phase of PEO/ORC blends; (c) MWCNT migrates from the PEO phase to the ORC phase one by one; (d) migration of MWCNTs completes; (e) the PEO phase is selectively removed using water; (f) R-ORC/MWCNT composites with a homogenous dispersion of MWCNTs in ORC matrix obtained by re-melting process.

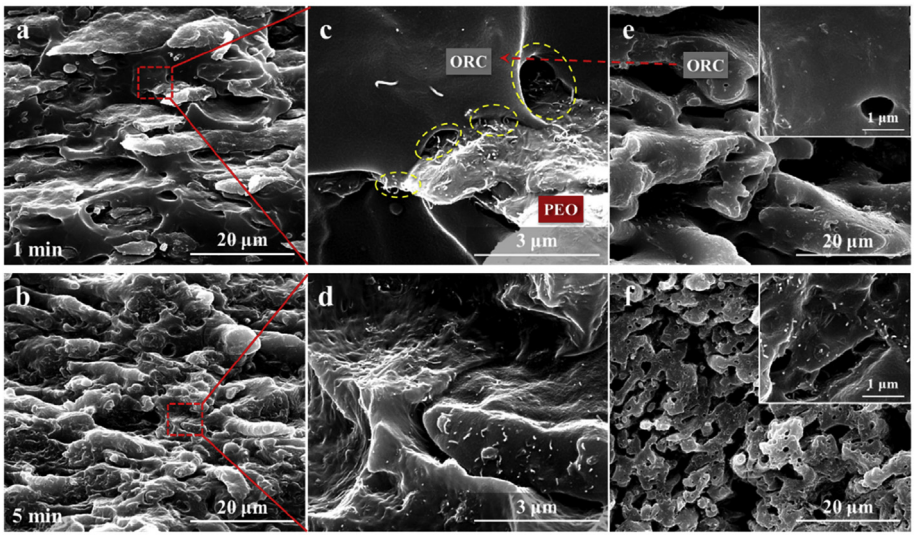

Fig. 3. The SEM micrographs of PEO/ORC/MWCNT-2.04 vol% composite experienced a melt compounding time of (a) 1 min and (b) 5 min. Image (c) and (d) are the amplification of image (a) and (b), respectively. Image (e) and (f) are the SEM micrographs of PEO/ORC/MWCNT-2.04 vol% with the PEO phase etched by deionized water after melt compounding for 1 min and 5 min, respectively.

between PEO and ORC becomes more and more blurry due to the improved compatibility and the interaction between the two phases during migration. It is clear that the fracture surface of the PEO phase is smooth and no MWCNTs can be found. Inversely, many single MWCNTs can be distinctly observed and homogeneously dispersed in the ORC phase. This result indicates that, as expected, MWCNTs can completely migrate from the PEO phase to the ORC phase after melt compounding for 15min.

In order to confirm the distribution and dispersion of MWCNTs in PEO/ORC/MWCNT composites, the SEM micrographs of PEO/ORC/MWCNT composites with PEO etched by water were taken and shown in Fig. 4b, d and f. After the PEO phase was selectively removed, there were only MWCNTs and ORC in the composites, and the composites showed a continuous porous structure. Compared with conventional melt compounded ORC/MWCNT composites shown in Fig. 1, it is obvious that no huge MWCNTs aggregation exists in the ORC matrix of the porous ORC/MWCNT composites as shown in Fig. 4b. What is more, in Fig. 4d and f, an extremely homogenous dispersion of MWCNTs in ORC can be observed and many single MWCNTs are visible. Combined with Fig. 4e and f, it can be confirmed that, consistent with the designed strategy shown in Fig. 2, MWCNTs can completely migrated from the PEO phase to the ORC phase during melt compounding and the extremely homogenous of MWCNTs in the PEO phase can be transferred to the ORC phase by this migration process. At last, a uniform dispersion of MWCNTs in the ORC phase can be achieved through the migration process of MWCNTs in PEO/ORC blends.

Thus, R-ORC/MWCNT composites with homogenously dispersed MWNCTs can be obtained by compressing the porous ORC/MWCNT composites at 140 °C for 5 min and the SEM micrographs of these samples are given in Fig. 5. Compared with conventional melt compounded ORC/MWCNT composites in Fig. 1, many single MWCNTs are visible at high magnification and no visible MWCNTs clusters can be observed at low magnification in R-ORC/MWCNT composites. As expected, after re-melting process, MWCNTs did not reunite into aggregates but maintained the homogenous dispersion state in R-ORC/MWCNT composites. All of these results manifest that the dispersion of MWCNTs in ORC matrix can be significantly improved by controlling the migration process of MWCNTs in PEO/ORC/MWCNT composites.

TEM observation was carried out to reveal the dispersion of MWCNTs visually at a more microcosmic scale. Fig. 6 shows the

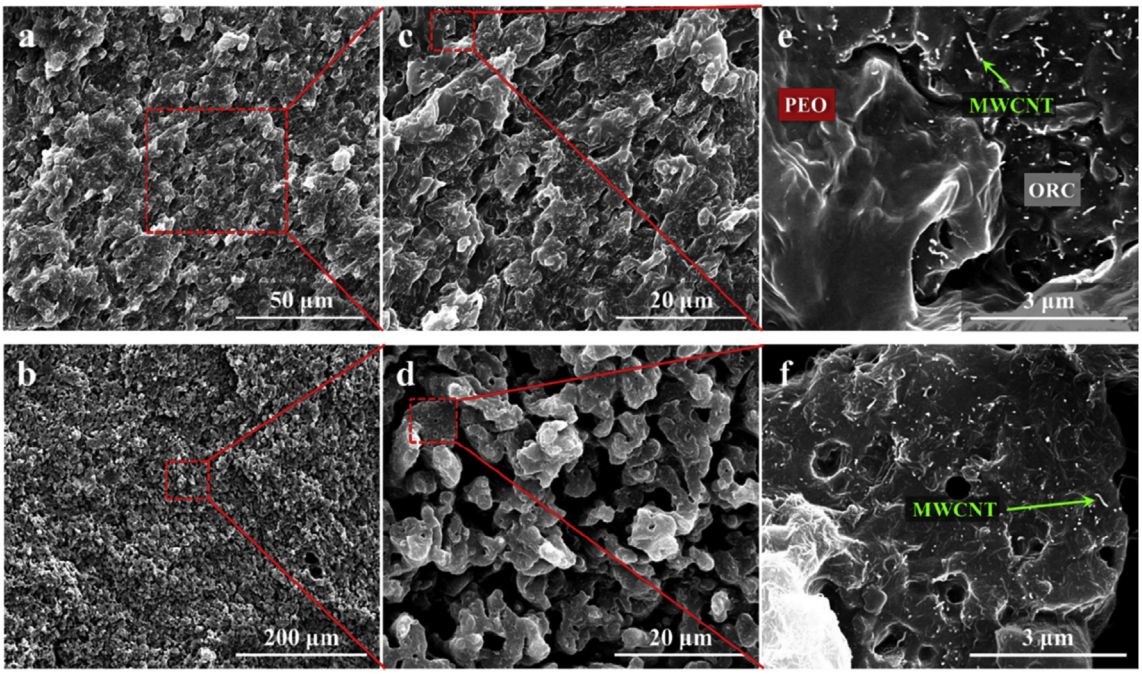

Fig. 4. SEM micrographs of (a) PEO/ORC/MWCNT-2.04 vol% experienced 15 min melt compounding and (b) PEO/ORC/MWCNT-2.04 vol% with PEO etched by water after 15 min melt compounding. Image (c), (e) and (d), (f) are the amplification of image (a) and (b), respectively.

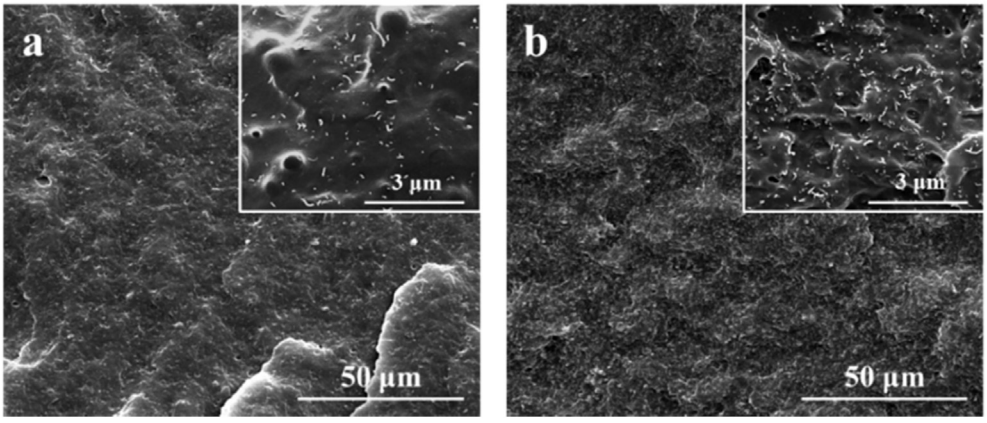

Fig. 5. The SEM micrographs of R-ORC/MWCNT composites. (a) R-ORC/MWCNT-1.75 vol% and (b) R-ORC/MWCNT-5.51 vol%. The inserts are the magnified images of each micrograph.

TEM micrographs of ORC/MWCNT and R-ORC/MWCNT composites with a MWCNT content of 1.75 vol% and the dark line represents MWCNTs distributed in the matrix. As shown in Fig. 6a, c and e, MWCNTs in ORC/MWCNT composites are not well dispersed and serious aggregations of MWCNTs can be observed. Besides, only very few MWCNTs can be found in the MWCNTs sparse regions. However, in R-ORC/MWCNT composites, homogenous dispersion of MWCNTs can be observed in the whole scope and almost all MWCNTs can maintain the form of isolated nanotubes, as shown in Fig. 6b, d and f. These results agree well with SEM observation and suggest that it is an effective approach to improve the dispersion of MWCNTs in ORC matrix by controlling the migration process of MWCNTs in PEO/ORC/MWCNT composites.

3.4. Rheological properties

Rheological measurements have been used to analyze the nanoparticle network in polymer/nano-filler system due to the suppression of nanoparticles network on the large-scale polymer relaxations [56]. To determine the existence and microstructure of the MWCNT network in both ORC/MWCNT and R-ORC/MWCNT composites, oscillatory shear rheological measurements were carried out at 140 °C and the results are shown in Fig. 7.

In Fig. 7a, it can be observed that the storage modulus (G') of pure ORC increases with the increase of frequency and shows a typical frequency dependence. With increasing the content of MWCNTs, the storage modulus increases and the slopes of the storage modulus curve at low frequencies decrease for both ORC/MWCNT and R-ORC/MWCNT composites. This distinct nonterminal behavior (At low frequencies, neat polymer chains can relax fully and exhibit the typical terminal behavior with the scaling law of approximate $G' \propto \omega^2$ and $G'' \propto \omega$. With the forming of rheological network, the relaxation of polymer chains will be suppressed and the slopes of the modulus curves of the samples at low frequency will decrease. This behavior is called nonterminal behavior.) for the two kinds of composites can be ascribed to the formed MWCNT

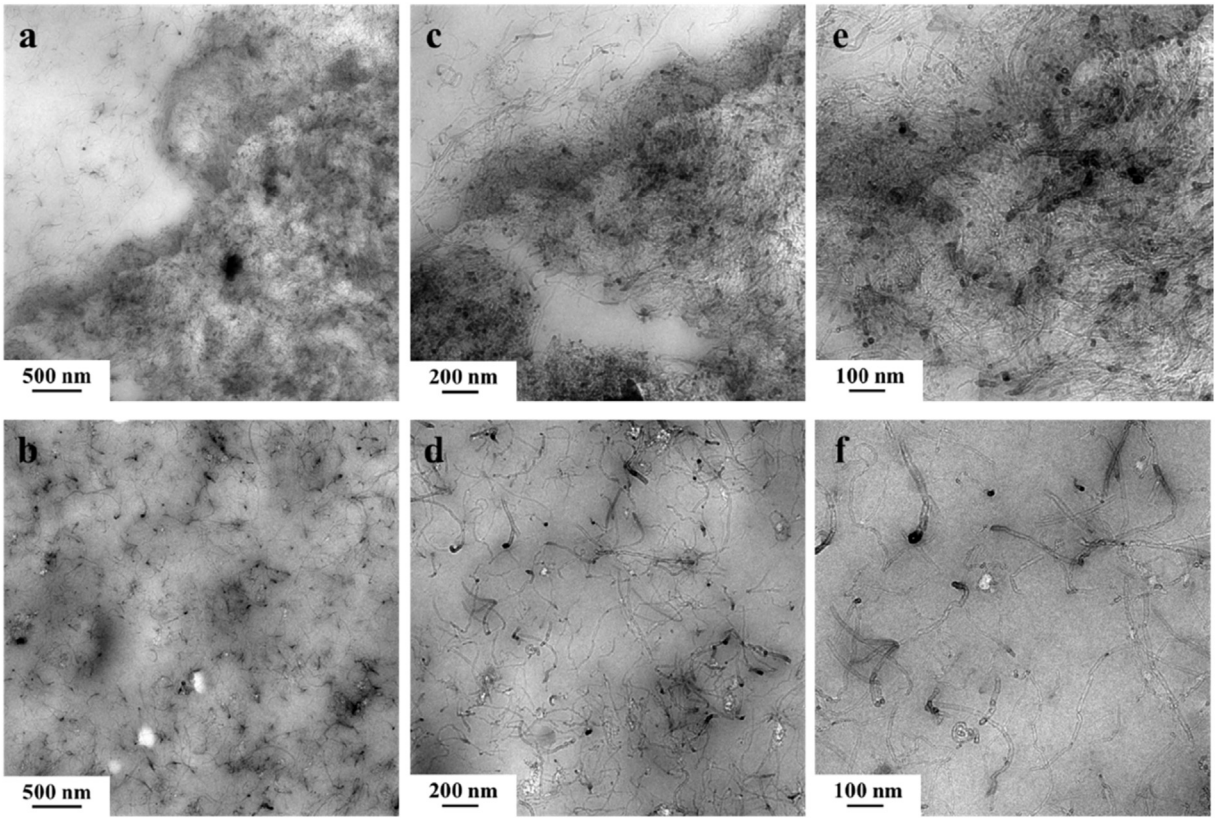

Fig. 6. The TEM micrographs of (a) ORC/MWCNT-1.75 vol% and (b) R-ORC/MWCNT-1.75 vol%. Image (c), (e) and (d), (f) are the amplification of image (a) and (b), respectively.

network, which significantly restrains the long-range motion of the polymer chains. When the loading of MWCNTs is relatively high (7.53 vol%), the storage modulus of both series of composites is almost independent of the frequency at low frequencies, indicating that the viscoelasticity of the materials has transformed to solid-like from liquid-like behavior because of the high intensity of MWCNT network.

It is worth noting that the storage modulus of R-ORC/MWCNT composites is always higher than that of ORC/MWCNT composites at the same content of MWCNTs and the same frequency, and the storage modulus plateau at low frequency is more evident in R-ORC/MWCNT composites. When the MWCNT concentration is only 0.86 vol%, for R-ORC/MWCNT composites, an obvious increase of storage modulus at low frequency can be observed and the slope derived in the low frequency terminal region of the lgG'-lgω curve is 0.45. Nevertheless, the storage modulus of ORC/MWCNT-0.86 is only a little higher than that of pure ORC, and the slope of the lgG'-lgω curve in the low frequency is 0.82. These results expressly reflect a more effective restraint of the large-scale polymer relaxation in R-ORC/MWCNT composites, indicating that the network of nanotubes is better developed due to the homogenous dispersion of MWCNTs in R-ORC/MWCNT composites.

The loss tangent (tan $\delta = G''/G'$) is an essential parameter to characterize the viscoelasticity of a material and is regarded more sensitive to the relaxation changes than G' and G'' [57]. A lower value of tan δ means that the viscoelasticity behavior of materials performs relatively more solid like [58]. Fig. 7b gives the relationship between tan δ for both series of composites with different contents of MWCNT and frequency. It can be seen that tan δ of pure ORC decreases with increasing the frequency, which is a typical behavior for viscoelastic liquid. Compared with pure ORC, both ORC/MWCNT and R-ORC/MWCNT composites exhibit a lower tan δ. In addition, at the same MWCNT concentration, the tan δ of R-ORC/MWCNT composites is always lower than that of ORC/MWCNT composites. Particularly, the tan δ of R-ORC/MWCNT-0.86 is almost lower than 1, while the tan δ of ORC/MWCNT-0.86 is much higher than 1 and only slightly lower than that of pure ORC in the low frequency range, suggesting a more densely packed MWCNT network in the R-ORC/MWCNT composites. These results also indicate that the MWCNT network of R-ORC/MWCNT composites is better developed at a lower content of MWCNT due to a homogenous dispersion of MWCNTs.

3.5. Electrical properties

Fig. 8a depicts the electrical conductivity of ORC/MWCNT composites and R-ORC/MWCNT composites as a function of volume content of MWCNTs. The conductivity for both ORC and R-ORC composites increases with increasing the content of MWCNTs. In comparison to ORC/MWCNT composites, R-ORC/MWCNT composites display a significantly higher electrical conductivity throughout the whole testing range.

Usually, the conductivity of filled polymer composites can be rationalized in terms of modified classical percolation theory [59], shown in equation (3):

$$\sigma = \sigma_0(\varphi - \varphi_c)^t \tag{3}$$

where σ is the conductivity of the composites, σ_0 is a scaling factor, φ is the volume fraction of the filler, φ_c is the threshold of the electrical conductivity percolation, t is the critical exponent revealing the dimensionality of the conductive networks.

The electrical conductivity percolation threshold, φ_c, of both series composites can be determined by fitting with the classical

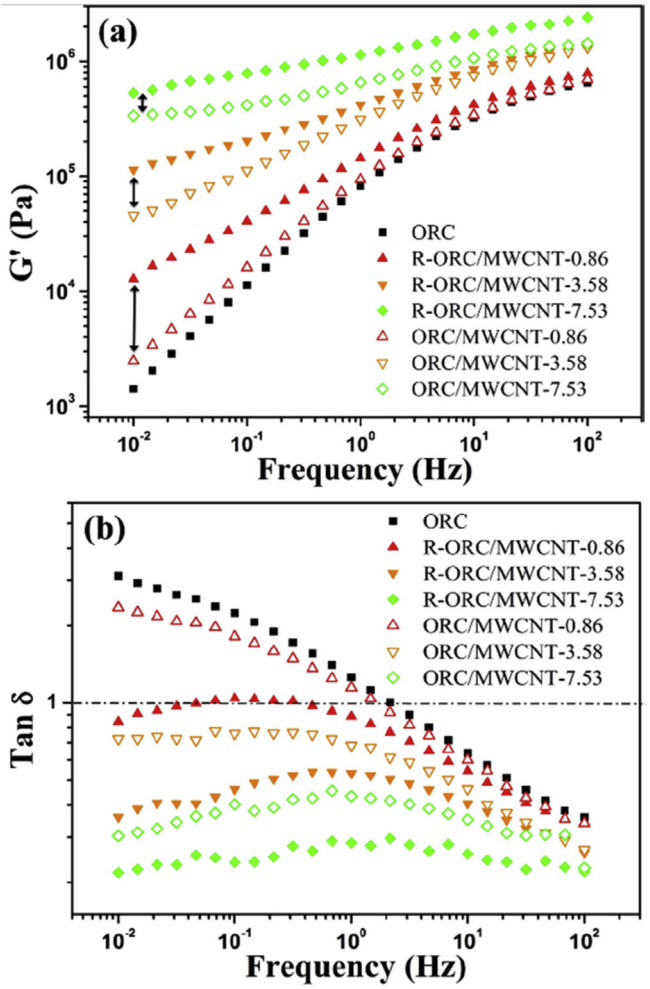

Fig. 7. Logarithmic plots of the (a) storage modulus and (b) loss tangent (tan δ) of pure ORC, ORC/MWCNT composites and R-ORC/MWCNT composites as a function of frequency at 140 °C.

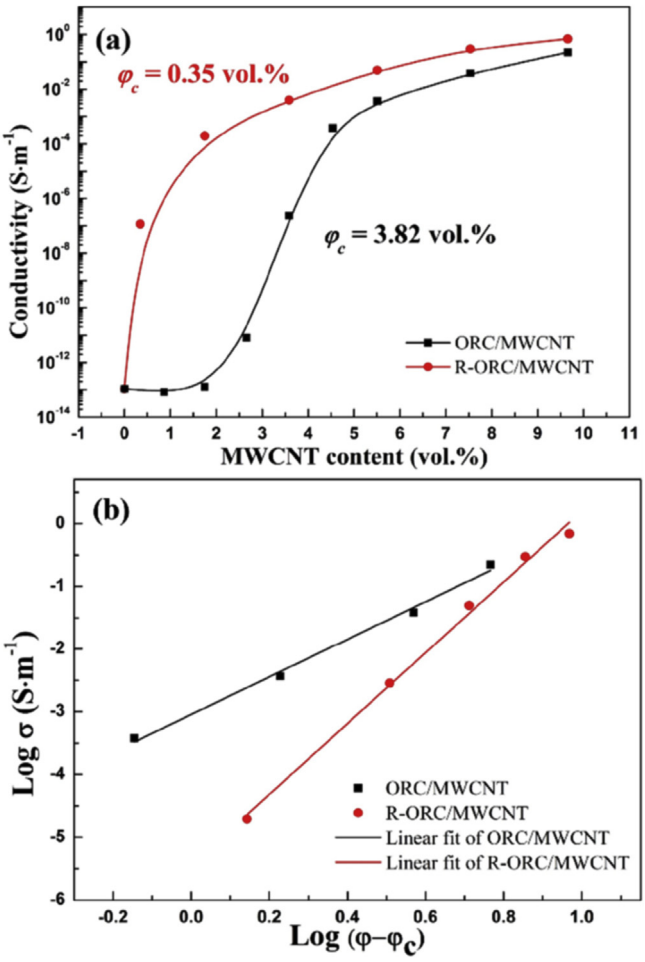

Fig. 8. (a) Dependence of resistivity on the content of MWCNT for ORC/MWCNT composites and R-ORC/MWCNT composites and (b) the fitted results of experimental results according to percolation theory.

percolation theory [18] to the experimentally obtained conductivity, as shown in Fig. 8b. The percolation threshold of ORC/MWCNT composites was calculated to be about 3.82 vol%, consistent with literature report [60]. Nevertheless, in R-ORC/MWCNT composites, the electrical conductivity percolation threshold is only about 0.35 vol%, approximately ten times lower than that of ORC/MWCNT composites.

As is known, factors including the aspect ratio of CNTs, disentanglement of CNT agglomerates, and the dispersion level of individual CNTs or CNT agglomerates, determine the percolation threshold of polymer/CNT nanocomposites [17,44]. When comparing Figs. 1 and 5, the percolation threshold of R-ORC/MWCNT composites is significantly decreased and the conductivity is tremendously improved, due to the uniform dispersion of MWCNTs in R-ORC/MWCNT composites, acquired by controlling the migration process of MWCNTs in PEO/ORC/MWCNT composites.

3.6. Mechanical properties

Many factors influence the mechanical properties of polymer/MWCNT composites, such as the aspect ratio of CNTs, dispersion states and the interfacial adhesion between CNTs and polymer matrix [61]. Since the matrix and MWCNTs in these two series of elastomeric composites are the same, so the dispersion level of MWCNTs is the pivotal influential factor. The SEM micrographs and representative uniaxial tensile stress-strain curves for both ORC/MWCNT composites and R-ORC/MWCNT composites were shown in Figs. S2 and S3.

The average values of important mechanical parameters are plotted *versus* the content of MWCNTs in Fig. 9. The tensile stress at 100% and 300% stretching of ORC/MWCNT composites and R-ORC/MWCNT composites at different MWCNT loadings was illustrated in Fig. 9a and b. Apparently, the tensile stress at 100% and 300% stretching is considerably improved for both series of elastomeric composites with increasing the content of MWCNTs. Moreover, due to the more uniform dispersion [44], the enhancement effect of MWCNTs on R-ORC/MWCNT composites is obviously better than that on ORC/MWCNT composites, and more effective reinforcing effect of MWCNTs. Fig. 9c shows the tensile modulus of ORC/MWCNT composites and R-ORC/MWCNT composites. The reinforcement of MWCNTs on the stiffness of composites is evident. What is more, compared with ORC/MWCNT composites at the same content of MWCNTs, the tensile modulus of R-ORC/MWCNT composites was increased by more than 25%, after improving the dispersion of MWCNT.

Fig. 9d displays the tensile elongation at break of the composites with different MWCNT contents. For the ORC/MWCNT composites, there is a sharp decrease of the elongation at break with increasing the content of MWCNT because of the existence of MWCNT

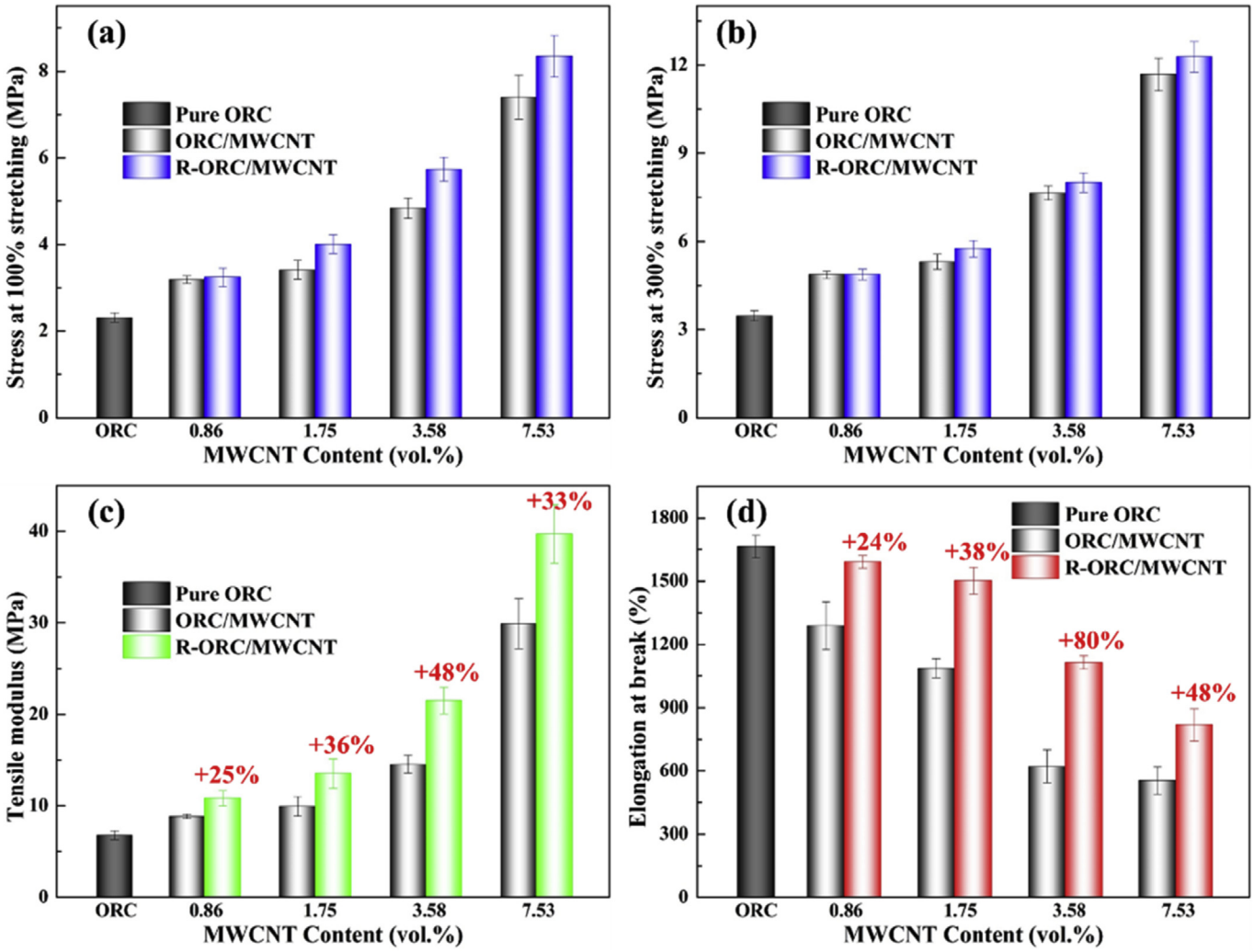

Fig. 9. (a) Stress at 100% stretching. (b) stress at 300% stretching. (c) tensile modulus and (d) elongation at break of pure ORC, ORC/MWCNT composites and R-ORC/MWCNT composites. Percentages in (c) and (d) are the percentages of reinforcement in the tensile modulus and elongation at break of R-ORC/MWCNT composites compared with ORC/MWCNT composites.

agglomerations which can lead to serious stress concentration when the material was subjected to an external force. Conversely, the elongation of R-ORC/MWCNT composites is at least 24% larger than that of ORC/MWCNT composites with the same content of MWCNTs. This is because the uniform dispersion of MWCNTs is beneficial for the efficient load transfer to the nanotube network [62] and this also results in a more uniform stress distribution and minimizes the presence of stress concentration centers [57].

4. Conclusion

A homogenous dispersion of MWCNTs in ORC matrix was obtained by thermodynamically and kinetically controlled migration of MWCNTs in PEO/ORC blends. The SEM micrographs showed that MWCNTs can completely migrate from the PEO phase to the ORC phase during melt compounding. Besides, MWCNTs can hold the form of isolated nanotubes during the whole migration process and a uniform dispersion of MWCNTs in ORC matrix can be eventually achieved after selectively removing the PEO phase. The rheological analysis revealed that after improving the dispersion of MWCNTs in ORC matrix, the MWCNTs network is better developed with a lower nanotube content due to a more uniform dispersion. As a result, the percolation threshold of ORC/MWCNT composites is significantly decreased and the electrical conductivity is tremendously improved. At the same time, due to the uniform MWCNTs dispersion, the mechanical properties were also fully enhanced compared with traditional melt compounded ORC/MWCNT composites. In summary, these results show that the dispersion of MWCNTs in the polymer matrix (especially for those generally get a poor dispersion of MWCNTs) can be significantly improved by proper selection of components with a selective distribution of MWCNTs and controlling the migration process of MWCNTs in the composites, and thus enhance the electrical and mechanical performance of polymer composites.

Acknowledgments

This work was funded by the National Natural Science Foundation of China (NNSFC Grant Nos. 51422305 and 51421061), Major State Basic Research Development Program of China (973 program) (Grant No. 2012CB025902), Here, please change “the Innovation Team Program of Science & Technology Department of Sichuan Province (Grant 2014TD0002)” into “Sichuan Provincial Science Fund for Distinguished Young Scholars (2015JQO003)”. Thank you.

Sichuan Provincial Science Fund for Distinguished Young Scholars (2015JQO003) and State Key Laboratory of Polymer Materials Engineering (Grant No. sklpme2014-2-02).

Appendix A. Supplementary data

Supplementary data related to this article can be found at http://dx.doi.org/10.1016/j.polymer.2016.12.056.

References

[1] X. Guan, G. Zheng, K. Dai, C. Liu, X. Yan, C. Shen, Z. Guo, Carbon Nanotubes-Adsorbed Electrospun PA66 Nanofiber Bundles with Improved Conductivity and Robust Flexibility, ACS Appl. Mat. Interfaces 8 (22) (2016) 14150–14159.
[2] B. Krause, R. Boldt, L. Häußler, P. Pötschke, Ultralow percolation threshold in polyamide 6.6/MWCNT composites, Compos. Sci. Technol. 114 (2015) 119–125.
[3] S. Biswas, G.P. Kar, S. Bose, Engineering nanostructured polymer blends with controlled nanoparticle location for excellent microwave absorption: a compartmentalized approach, Nanoscale 7 (26) (2015) 11334–11351.
[4] T. Li, L.-F. Ma, R.-Y. Bao, G.-Q. Qi, W. Yang, B.-H. Xie, M.-B. Yang, A new approach to construct segregated structures in thermoplastic polyolefin elastomers towards improved conductive and mechanical properties, J. Mat. Chem. A 3 (10) (2015) 5482–5490.
[5] Y. He, W. Chen, C. Gao, J. Zhou, X. Li, E. Xie, An overview of carbon materials for flexible electrochemical capacitors, Nanoscale 5 (19) (2013) 8799–8820.
[6] H. Gu, C. Ma, J. Gu, J. Guo, X. Yan, J. Huang, Q. Zhang, Z. Guo, An overview of multifunctional epoxy nanocomposites, J. Mat. Chem. C 4 (25) (2016) 5890–5906.
[7] H. Lee, J.-K. Yoo, J.-H. Park, J.H. Kim, K. Kang, Y.S. Jung, A Stretchable Polymer–Carbon Nanotube Composite Electrode for Flexible Lithium-Ion Batteries: Porosity Engineering by Controlled Phase Separation, Adv. Energy Mater 2 (8) (2012) 976–982.
[8] H. Liu, J. Gao, W. Huang, K. Dai, G. Zheng, C. Liu, C. Shen, X. Yan, J. Guo, Z. Guo, Electrically conductive strain sensing polyurethane nanocomposites with synergistic carbon nanotubes and graphene bifillers, Nanoscale 8 (2016) 12977–12989.
[9] J. Huang, Y. Zhu, W. Jiang, Q. Tang, Parallel carbon nanotube stripes in polymer thin film with tunable microstructures and anisotropic conductive properties, Compos. Part A-Appl. S 69 (2015) 240–246.
[10] Y. Wei, Z. Li, X. Liu, K. Dai, G. Zheng, C. Liu, J. Chen, C. Shen, Temperature-resistivity characteristics of a segregated conductive CB/PP/UHMWPE composite, Colloid Polym. Sci. 292 (11) (2014) 2891–2898.
[11] Y.-S. Ye, H.-X. Zeng, J. Wu, L.-Y. Dong, J.-T. Zhu, Z.-G. Xue, X.-P. Zhou, X.-L. Xie, Y.-W. Mai, Biocompatible reduced graphene oxide sheets with superior water dispersibility stabilized by cellulose nanocrystals and their polyethylene oxide composites, Green Chem. 18 (6) (2016) 1674–1683.
[12] N. Domun, H. Hadavinia, T. Zhang, T. Sainsbury, G.H. Liaghat, S. Vahid, Improving the fracture toughness and the strength of epoxy using nanomaterials–a review of the current status, Nanoscale 7 (23) (2015) 10294–10329.
[13] Y. Liu, S. Kumar, Polymer/carbon nanotube nano composite fibers–a review, ACS Appl. Mat. Interfaces 6 (9) (2014) 6069–6087.
[14] N. Grossiord, J. Loos, O. Regev, C.E. Koning, Toolbox for Dispersing Carbon Nanotubes into Polymers To Get Conductive Nanocomposites, Chem. Mater 18 (5) (2006) 1089–1099.
[15] E.T. Thostenson, Z. Ren, T.-W. Chou, Advances in the science and technology of carbon nanotubes and their composites: a review, Compos. Sci. Technol. 61 (13) (2001) 1899–1912.
[16] G. Keledi, J. Hari, B. Pukanszky, Polymer nanocomposites: structure, interaction, and functionality, Nanoscale 4 (6) (2012) 1919–1938.
[17] X. Xie, Y. Mai, X. Zhou, Dispersion and alignment of carbon nanotubes in polymer matrix: A review, Mat. Sci. Eng. R. 49 (4) (2005) 89–112.
[18] Z. Spitalsky, D. Tasis, K. Papagelis, C. Galiotis, Carbon nanotube–polymer composites: Chemistry, processing, mechanical and electrical properties, Prog. Polym. Sci. 35 (3) (2010) 357–401.
[19] M.B. Bryning, M.F. Islam, J.M. Kikkawa, A.G. Yodh, Very Low Conductivity Threshold in Bulk Isotropic Single-Walled Carbon Nanotube–Epoxy Composites, Adv. Mater 17 (9) (2005) 1186–1191.
[20] Y. Li, H. Shimizu, Toward a Stretchable, Elastic, and Electrically Conductive Nanocomposite: Morphology and Properties of Poly[styrene-b-(ethylene-co-butylene)-b-styrene]/Multiwalled Carbon Nanotube Composites Fabricated by High-Shear Processing, Macromolecules 42 (7) (2009) 2587–2593.
[21] S. Roy, T. Das, Y. Ming, X. Chen, C.Y. Yue, X. Hu, Specific functionalization and polymer grafting on multiwalled carbon nanotubes to fabricate advanced nylon 12 composites, J. Mat. Chem. A 2 (11) (2014) 3961.
[22] H. Gu, S. Tadakamalla, X. Zhang, Y. Huang, Y. Jiang, H.A. Colorado, Z. Luo, S. Wei, Z. Guo, Epoxy resin nanosuspensions and reinforced nanocomposites from polyaniline stabilized multi-walled carbon nanotubes, J. Mat. Chem. C 1 (4) (2013) 729–743.
[23] M.F. Islam, E. Rojas, D.M. Bergey, A.T. Johnson, A.G. Yodh, High Weight Fraction Surfactant Solubilization of Single-Wall Carbon Nanotubes in Water, Nano Lett. 3 (2) (2003) 269–273.
[24] D. Wang, H. Li, M. Li, H. Jiang, M. Xia, Z. Zhou, Stretchable conductive polyurethane elastomer in situ polymerized with multi-walled carbon nanotubes, J. Mat. Chem. C 1 (15) (2013) 2744.
[25] N. Hameed, N.V. Salim, T.L. Hanley, M. Sona, B.L. Fox, Q. Guo, Individual dispersion of carbon nanotubes in epoxy via a novel dispersion-curing approach using ionic liquids, Phys. Chem. Chem. Phys. 15 (28) (2013) 11696–11703.
[26] A. Prevoteau, C. Soulie-Ziakovic, L. Leibler, Universally dispersible carbon nanotubes, J. Am. Chem. Soc. 134 (49) (2012) 19961–19964.
[27] T. Gong, S.-P. Peng, R.-Y. Bao, W. Yang, B.-H. Xie, M.-B. Yang, Low percolation threshold and balanced electrical and mechanical performances in polypropylene/carbon black composites with a continuous segregated structure, Compos. Part B Eng. 99 (2016) 348–357.
[28] B. Du, U.A. Handge, M. Wambach, C. Abetz, S. Rangou, V. Abetz, Functionalization of MWCNT with P(MMA-co-S) copolymers via ATRP: Influence on localization of MWCNT in SAN/PPE 40/60 blends and on rheological and dielectric properties of the composites, Polymer 54 (22) (2013) 6165–6176.
[29] A. Taguet, P. Cassagnau, J.M. Lopez-Cuesta, Structuration, selective dispersion and compatibilizing effect of (nano)fillers in polymer blends, Prog. Polym. Sci. 39 (8) (2014) 1526–1563.
[30] F. Fenouillot, P. Cassagnau, J.C. Majesté, Uneven distribution of nanoparticles in immiscible fluids: Morphology development in polymer blends, Polym. 50 (6) (2009) 1333–1350.
[31] J. Chen, H.-y. Lu, J.-h. Yang, Y. Wang, X.-t. Zheng, C.-l. Zhang, G.-p. Yuan, Effect of organoclay on morphology and electrical conductivity of PC/PVDF/CNT blend composites, Compos. Sci. Technol. 94 (2014) 30–38.
[32] Z.-Y. Xiong, L. Wang, Y. Sun, Z.-X. Guo, J. Yu, Migration of MWCNTs during melt preparation of ABS/PC/MWCNT conductive composites via PC/MWCNT masterbatch approach, Polymer 54 (1) (2013) 447–455.
[33] J. Huang, C. Mao, Y. Zhu, W. Jiang, X. Yang, Control of carbon nanotubes at the interface of a co-continuous immiscible polymer blend to fabricate conductive composites with ultralow percolation thresholds, Carbon 73 (2014) 267–274.
[34] A. Göldel, A. Marmur, G.R. Kasaliwal, P. Pötschke, G. Heinrich, Shape-Dependent Localization of Carbon Nanotubes and Carbon Black in an Immiscible Polymer Blend during Melt Mixing, Macromolecules 44 (15) (2011) 6094–6102.
[35] A. Goldel, G. Kasaliwal, P. Pötschke, Selective Localization and Migration of Multiwalled Carbon Nanotubes in Blends of Polycarbonate and Poly(styrene-acrylonitrile), Macromol. Rapid Commun. 30 (6) (2009) 423–429.
[36] A. Göldel, G.R. Kasaliwal, P. Pötschke, G. Heinrich, The kinetics of CNT transfer between immiscible blend phases during melt mixing, Polymer 53 (2) (2012) 411–421.
[37] L.-F. Ma, R.-Y. Bao, R. Dou, S.-D. Zheng, Z.-Y. Liu, R.-Y. Zhang, M.-B. Yang, W. Yang, Conductive thermoplastic vulcanizates (TPVs) based on polypropylene (PP)/ethylene-propylene-diene rubber (EPDM) blend: From strain sensor to highly stretchable conductor, Compos. Sci. Technol. 128 (2016) 176–184.
[38] H.J. Salavagione, S. Quiles-Díaz, P. Enrique-Jimenez, G. Martínez, F. Ania, A. Flores, M.A. Gómez-Fatou, Development of Advanced Elastomeric Conductive Nanocomposites by Selective Chemical Affinity of Modified Graphene, Macromolecules 49 (13) (2016) 4948–4956.
[39] S. Yao, Y. Zhu, Nanomaterial-enabled stretchable conductors: strategies, materials and devices, Adv. Mater 27 (9) (2015) 1480–1511.
[40] A.T. Sepulveda, R. Guzman de Villoria, J.C. Viana, A.J. Pontes, B.L. Wardle, L.A. Rocha, Full elastic constitutive relation of non-isotropic aligned-CNT/PDMS flexible nanocomposites, Nanoscale 5 (11) (2013) 4847–4854.
[41] A.G. Simanke, G.B. Galland, L. Freitas, J.A.H. da Jornada, R. Quijada, R.S. Mauler, Influence of the comonomer content on the thermal and dynamic mechanical properties of metallocene ethylene/1-octene copolymers, Polymer 40 (20) (1999) 5489–5495.
[42] O. Osazuwa, K. Petrie, M. Kontopoulou, P. Xiang, Z. Ye, A. Docoslis, Characterization of non-covalently, non-specifically functionalized multi-wall carbon nanotubes and their melt compounded composites with an ethylene–octene copolymer, Compos. Sci. Technol. 73 (2012) 27–33.
[43] I.L. Hosier, R.G. Alamo, P. Esteso, J.R. Isasi, L. Mandelkern, Formation of the α and γ Polymorphs in Random Metallocene–Propylene Copolymers, Eff. Concentration Type Comonomer, Macromol. 36 (15) (2003) 5623–5636.
[44] T. Li, J.-H. Pu, L.-F. Ma, R.-Y. Bao, G.-Q. Qi, W. Yang, B.-H. Xie, M.-B. Yang, An extremely uniform dispersion of MWCNTs in olefin block copolymers significantly enhances electrical and mechanical performances, Polym. Chem. 6 (40) (2015) 7160–7170.
[45] M. Shaheer Akhtar, J.-G. Park, H.-C. Lee, S.K. Lee, O.B. Yang, Carbon nanotubes–polyethylene oxide composite electrolyte for solid-state dye-sensitized solar cells, Electrochimica Acta 55 (7) (2010) 2418–2423.
[46] M. Park, H. Kim, J.P. Youngblood, S.W. Han, E. Verplogen, A.J. Hart, Excellent dispersion of MWCNTs in PEO polymer achieved through a simple and potentially cost-effective evaporation casting, Nanotechnology 22 (41) (2011) 415703.
[47] J. Chen, X.-C. Du, W.-B. Zhang, J.-H. Yang, N. Zhang, T. Huang, Y. Wang, Synergistic effect of carbon nanotubes and carbon black on electrical conductivity of PA6/ABS blend, Compos. Sci. Technol. 81 (2013) 1–8.
[48] S.P. Pawar, S. Bose, Peculiar morphological transitions induced by nanoparticles in polymeric blends: retarded relaxation or altered interfacial

tension? Phys. Chem. Chem. Phys. 17 (22) (2015) 14470–14478.
[49] M. Sumita, K. Sakata, S. Asai, K. Miyasaka, H. Nakagawa, Dispersion of fillers and the electrical conductivity of polymer blends filled with carbon black, Polym. Bull. 25 (2) (1991) 265–271.
[50] S. Wu, Interfacial and Surface Tensions of Polymers, J. Macromol. Sci. C. Rev. Macromol. Chem. 10 (1) (1974) 1–73.
[51] R. Cardinaud, T. McNally, Localization of MWCNTs in PET/LDPE blends, Eur. Polym. J. 49 (6) (2013) 1287–1297.
[52] A.-C. Baudouin, J. Devaux, C. Bailly, Localization of carbon nanotubes at the interface in blends of polyamide and ethylene–acrylate copolymer, Polymer 51 (6) (2010) 1341–1354.
[53] M. Trifkovic, A.T. Hedegaard, M. Sheikhzadeh, S. Huang, C.W. Macosko, Stabilization of PE/PEO Cocontinuous Blends by Interfacial Nanoclays, Macromolecules 48 (13) (2015) 4631–4644.
[54] M. Trifkovic, A. Hedegaard, K. Huston, M. Sheikhzadeh, C.W. Macosko, Porous Films via PE/PEO Cocontinuous Blends, Macromolecules 45 (15) (2012) 6036–6044.
[55] M. Pakravan, M.C. Heuzey, A. Ajji, Core-shell structured PEO-chitosan nanofibers by coaxial electrospinning, Biomacromolecules 13 (2) (2012) 412–421.
[56] C.-L. Huang, C. Wang, Rheological and conductive percolation laws for syndiotactic polystyrene composites filled with carbon nanocapsules and carbon nanotubes, Carbon 49 (7) (2011) 2334–2344.
[57] Z. Xu, Y. Niu, L. Yang, W. Xie, H. Li, Z. Gan, Z. Wang, Morphology, rheology and crystallization behavior of polylactide composites prepared through addition of five-armed star polylactide grafted multiwalled carbon nanotubes, Polymer 51 (3) (2010) 730–737.
[58] X.-F. Wei, R.-Y. Bao, Z.-Q. Cao, W. Yang, B.-H. Xie, M.-B. Yang, Stereocomplex Crystallite Network in Asymmetric PLLA/PDLA Blends: Formation, Structure, and Confining Effect on the Crystallization Rate of Homocrystallites, Macromolecules 47 (4) (2014) 1439–1448.
[59] B. Mathieu, C. Anthony, A. Arnaud, F. Lionel, CNT aggregation mechanisms probed by electrical and dielectric measurements, J. Mat. Chem. C 3 (22) (2015) 5769–5774.
[60] P. Slobodian, P. Riha, R. Olejnik, M. Kovar, P. Svoboda, Thermoelectric Properties of Carbon Nanotube and Nanofiber Based Ethylene-Octene Copolymer Composites for Thermoelectric Devices, J. Nanomater 2013 (2013) 1–7.
[61] J.N. Coleman, U. Khan, W.J. Blau, Y.K. Gun'ko, Small but strong: A review of the mechanical properties of carbon nanotube–polymer composites, Carbon 44 (9) (2006) 1624–1652.
[62] J.A. Kim, D.G. Seong, T.J. Kang, J.R. Youn, Effects of surface modification on rheological and mechanical properties of CNT/epoxy composites, Carbon 44 (10) (2006) 1898–1905.